Journal of Power Sources 520 (2022) 230883

Contents lists available at ScienceDirect

Journal of Power Sources

journal homepage: www.elsevier.com/locate/jpowsour

Bimetallic AC/Ag_2CrO_4/SnS heterostructure photoanode for energy conversion and storage: A self-powered Photocapacitor

Thirunavukarasu Kajana [a,b,c], Arumugam Pirashanthan [a,c], Akila Yuvapragasam [c], Dhayalan Velauthapillai [c,*], Punniamoorthy Ravirajan [a], Meena Senthilnanthanan [b,**]

[a] Clean Energy Research Laboratory, Department of Physics, University of Jaffna, 40000, Jaffna, Sri Lanka
[b] Department of Chemistry, University of Jaffna, 4000, Jaffna, Sri Lanka
[c] Faculty of Engineering and Science, Western Norway University of Applied Sciences, 5063, Bergen, Norway

HIGHLIGHTS

- A promising path for the design of efficient solar energy harvesting and storage.
- A novel photocapacitor with FTO/Activated Carbon/Ag_2CrO_4/SnS photoanode.
- The specific capacitance of 4782 mF/g (10 mVs^{-1}) at 1 sun illumination.
- Synthesis & photoelectrochemical application of rod-like Ag_2CrO_4 & flake-like SnS.

ARTICLE INFO

Keywords:
Photocapacitor
Energy storage
Photoanode
Activated carbon
Heterostructure
Cyclic voltammetry

ABSTRACT

The worldwide increase in generation of solar based electricity prompts the essentiality of research efforts on the development of energy storage systems. In this regard, self-powered photocapacitors are of keen interest as they can directly convert and store the solar energy in the form of electrical energy in a single device. This study reports the photoelectrochemical energy storage capacity of a novel photocapacitor fabricated with FTO/Activated Carbon (AC)/Ag_2CrO_4/SnS nanostructured photoanode. Initially, the Ag_2CrO_4 and SnS nanostructures were synthesized using simple ultrasonication technique and hydrothermal method, respectively. The crystallinity, morphology and optical properties of the synthesized nanostructures were then studied. The XRD patterns indicated orthorhombic structure of both Ag_2CrO_4 and SnS. Their optical band gaps were calculated as 1.93 and 1.65 eV, respectively using Kubelka-Munk plots. The FTO/AC/Ag_2CrO_4/SnS photoanode was then fabricated and photoelectrochemical studies, namely cyclic voltammetry and electrochemical impedance spectroscopy were carried out on a three electrode system. The FTO/AC/Ag_2CrO_4/SnS photoanode showed a specific capacitance of 4782 mF/g at the scan rate of 10 mVs^{-1} when the device was subjected to visible light illumination (1 sun). Hence, the fabricated heterostructured photoanode provides a promising path for the design and synthesis of novel highly efficient solar energy harvesting and storage materials as photocapacitors.

1. Introduction

Solar energy is virtually unlimited and regarded as the most essential need for the future compared with other energy resources such as wind, hydro power, tidal waves, geothermal and biomass [1]. The direct conversion of solar energy to electricity through Photoelectric Conversion technology has been recognized as one of the most effective and sustainable methods. Such electricity generation with solar cells is efficient and cost-effective [2–4]. Various solar cells have been developed to harvest solar energy efficiently, such as junction solar cells [5], dye-sensitized cells [6] and organometal halide perovskite cells (PSCs) [7]. However, the intermittence of solar energy makes it an unreliable source to fulfil the energy demand at all times [8–10]. The coupling of solar cells with energy storage devices is a promising strategy to

* Corresponding author.
** Corresponding author.
E-mail addresses: tskajana@gmail.com (T. Kajana), pirashanthan.arumugam@gmail.com (A. Pirashanthan), akilayuva@gmail.com (A. Yuvapragasam), Dhayalan.Velauthapillai@hvl.no (D. Velauthapillai), pravirajan@univ.jfn.ac.lk (P. Ravirajan), meena@univ.jfn.ac.lk (M. Senthilnanthanan).

https://doi.org/10.1016/j.jpowsour.2021.230883
Received 10 August 2021; Received in revised form 30 November 2021; Accepted 6 December 2021
Available online 11 December 2021

overcome this problem and is an effective way to utilize solar energy [11–13]. In general, the energy conversion and storage units in a solar energy production system operates independently, resulting in energy transfer from the conversion unit to the storage unit mediated by the external wire connections [14].

In recent decades, a new type of capacitor, known as 'Photocapacitor', which is a single device with two units for solar energy conversion and storage without the demand for external power sources is being studied and has attracted great attention for their potential applications in portable and wearable electronics [10,15,16]. Moreover, this kind of photocapacitor leads to 43% reduction in device internal resistance as compared to that of using external wire connection the photocapacitor. Miyasaka and Murakami constructed a simple sandwich-type electrochemical cell consisting of a light-absorbing electrode (photoelectrode) comprising dye-sensitized semiconductor nanoparticles/hole-trapping layer/activated carbon particles in contact with an organic electrolyte solution and they achieved a capacitance of 0.69 Fcm^{-2} [17]. Safshekan et al. developed a photocapacitive device based on the heterostructured $BiVO_4$-PbO_x system with a specific capacitance of 6 $mFcm^{-2}$ [18]. In Photocapacitors, photo active material plays a vital role since it undertakes the photoelectric conversion task. The design of Photocapacitor can reduce the resistive losses compared to conventional systems in which solar cells are coupled with batteries. Moreover, the performance of photo active materials is improved by enhancing separation and reducing recombination of charge carriers.

In recent times, silver-based compounds have gained attention owing to their morphology and structure with high electron transfer capability and visible light utilization rate, which make them promising candidates for various applications as Ag_2CrO_4 with a narrow band gap of about 1.8 eV is a novel Ag-based nanomaterial for degradation of dyes [19–22], hydrogen production [23] and sensors [24]. Unfortunately, the photocorrosion of Ag_2CrO_4 hinders its practical application [25,26]. It is necessary to construct heterojunction [27], or metal organic frameworks (MOFs) [28] with other semiconductors to improve stability and prevent photocorrosion of Ag_2CrO_4. Carbon satisfies these requirements at high scan rates and particularly with aqueous electrolytes; because it provides additional open surface area for energy storage and its highly porous nature results in improved performance with aqueous electrolytes.

Recently, our research group published a novel heterostructured carbon sheet/Ag_2MoO_4/SnS Photocapacitor with highest specific capacitance of 340 F/g with an open circuit potential of 1.25 V vs. Silver/Silver chloride reference electrode [29]. The reported high capacitance was due to the large specific area and high conductivity of the Ag_2MoO_4/SnS film. Here, Ag_2MoO_4 was served as photon absorbing layer and SnS was employed as an energy storage layer through facilitating the transformation of SnS to SnO_x during operation. This study focuses on Ag_2CrO_4 as the absorption layer due to the visible absorption of Ag_2CrO_4 which could be more effective than that of UV absorption of Ag_2MoO_4. Due to the difficulties with hydrothermal coating of Ag_2CrO_4 on ultra-smooth carbon sheet, the carbon sheet was replaced with transparent Fluorine-doped Tin Oxide (FTO) glass substrate and was used as highly conductive activated carbon (AC) to hold Ag_2CrO_4 on top FTO. Here we report the performance of another novel AC/Ag_2CrO_4/SnS heterostructure based Photocapacitor where both oxidative and reductive energies are effectively utilized by a single electrode under the illumination of solar energy. The core components of this device are Ag_2CrO_4/SnS heterostructured nanomaterials, in which Ag_2CrO_4 is employed as the photoactive core of a novel photocapacitive system to generate electrons and holes by absorbing solar radiation. The photogenerated holes are subsequently stored in a capacitive SnO_x layer. This storage stand is obtained through photo oxidation of SnS nanoparticles.

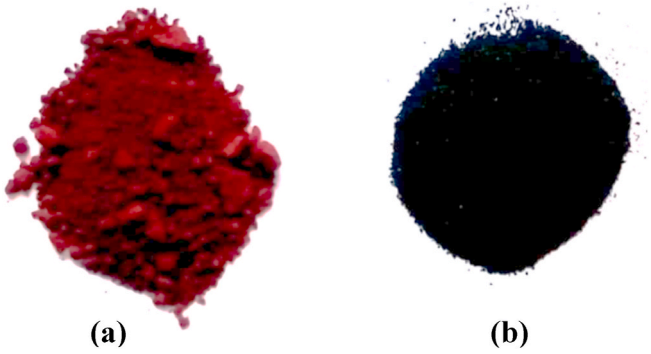

Fig. 1. Synthesized **(a)** Ag_2CrO_4 and **(b)** SnS powders.

2. Materials and methods

2.1. Materials

The chemicals, such as silver nitrate [$AgNO_3$, ≥99%], sodium chromate [Na_2CrO_4, 98%] sodium salicylate [$C_7H_5NaO_3$, 99.5%] and ethanol [C_2H_5OH, 99.99%] were used for the synthesis of silver chromate [Ag_2CrO_4] whereas tin(II) chloride dihydrate [$SnCl_2{\cdot}2H_2O$, 98%], thiourea [$CS(NH_2)_2$, ≥99.0%] and acetone [$(CH_3)_2CO$, ≥99.0%] were used for the synthesis of SnS. Polyvinylidene difluoride [PVDF, average M.W. 534,000] and dimethylformamide [DMF, ≥99.0%] were used as binders for electrode preparation. The phosphate buffer solution was prepared using disodium hydrogen phosphate [Na_2HPO_4, HPLC grade] and sodium dihydrogen phosphate [NaH_2PO_4, HPLC grade]. All the above chemicals were purchased from Sigma-Aldrich and used without further purification. The activated carbon (AC) was obtained from Nova Carbons India (Pvt.) Ltd.

2.2. Synthesis

2.2.1. Synthesis of Ag_2CrO_4 powder

In a typical synthesis of $C_7H_5AgO_3$ powder, initially, $AgNO_3$ and $C_7H_5NaO_3$ powders were dissolved in deionized water (DI water) separately. Then, the prepared $C_7H_5NaO_3$ solution was gradually added into the $AgNO_3$ solution with vigorous stirring for 30 min, which resulted in the formation of a white precipitate. As-synthesized white precipitate ($C_7H_5AgO_3$) was centrifuged, washed with DI water and ethanol several times and dried overnight at 50 °C in the oven.

The dried $C_7H_5AgO_3$ powder was dissolved in hot DI water under magnetic stirring for 15 min and then Na_2CrO_4 solution (Na_2CrO_4 dissolved in DI water) was sequentially introduced to the $C_7H_5AgO_3$ solution using a burette with continued stirring. The resulting reddish-brown coloured solution was ultrasonicated for 1 h. The obtained reddish-brown coloured precipitate was washed repeatedly with DI water and ethanol several times. Finally, the product was dried overnight at 50 °C to obtain Ag_2CrO_4 powder as shown in Fig. 1 (a).

2.2.2. Synthesis of SnS powder

A mixture of $SnCl_2{\cdot}2H_2O$ and thiourea, dissolved in DI water, was heated in an autoclave at 180 °C for 2 h and allowed to cool to room temperature naturally. Then, the reaction mixture was centrifuged, and the resulted black coloured precipitate was filtered, washed with DI water and dried at 120 °C to obtain the SnS powder as shown in Fig. 1 (b).

2.3. Fabrication of photoanode (working electrode): AC/Ag_2CrO_4/SnS

Initially, a mixture of AC and PVDF in the weight ratio of 9:1 was stirred for 6 h and the obtained slurry was doctor bladed on a clean FTO glass substrate. The FTO/AC films were dried at 120 °C for 2 h and then

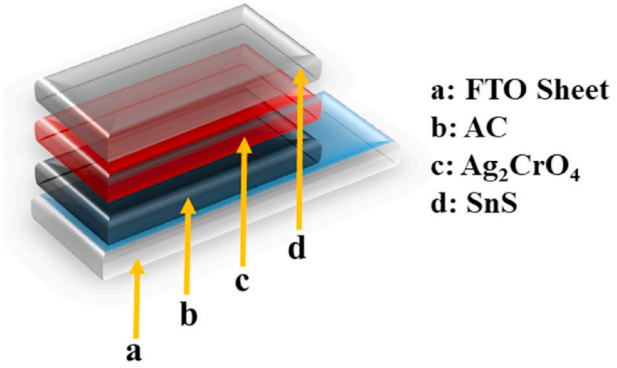

Fig. 2. Schematic diagram of the developed FTO/AC/Ag_2CrO_4/SnS photoanode.

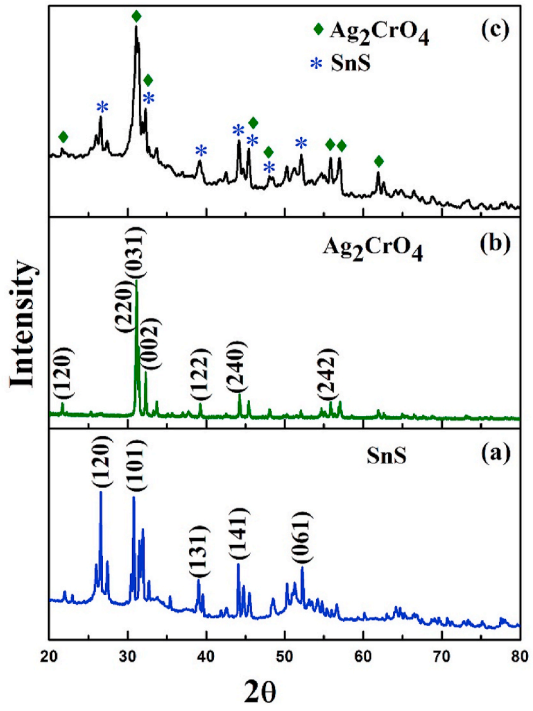

Fig. 3. XRD patterns of the prepared samples of **(a)** bare SnS **(b)** bare Ag_2CrO_4 and **(c)** Ag_2CrO_4/SnS on FTO/AC films.

kept immersed in the NaOH solution for 24 h to remove any impurities. Subsequently, a finely ground mixture of Ag_2CrO_4 and PVDF in the weight ratio of 3:1 was doctor bladed on the air dried FTO/AC film to deposit the Ag_2CrO_4 layer on the films. Finally, the SnS layer was deposited on the FTO/AC/Ag_2CrO_4 film using a mixture of SnS and PVDF in the weight ratio of 3:1 and adopting the same procedure to prepare the FTO/AC/Ag_2CrO_4/SnS electrode. The deposition of Ag_2CrO_4 and SnS layers was followed by drying in a furnace at 140 °C and 120 °C respectively. The schematic diagram of the developed FTO/AC/Ag_2CrO_4/SnS photoanode is shown in Fig. 2.

2.4. Photoelectrochemical properties

In order to investigate the photoelectrochemical properties of the working electrode of FTO/AC/Ag_2CrO_4/SnS, the cyclic voltammetry (CV) and electrochemical impedance spectroscopy (EIS) were carried out by using Bio Logic SP-150 potentiostat. Measurements were carried out with a three-electrode system and an aqueous solution buffered to pH 7 using a 0.1 M phosphate buffer solution as electrolyte. For

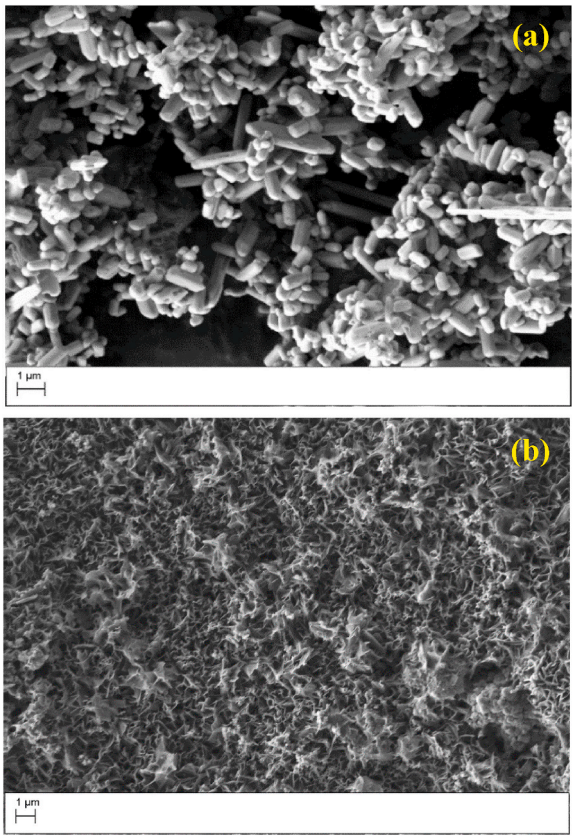

Fig. 4. SEM images of **(a)** Ag_2CrO_4 and **(b)** SnS on Ag_2CrO_4 coated FTO/AC films.

photoelectrochemical characterization, the electrodes were illuminated using a 150 Xenon lamp and the cyclic voltammetry was carried out in the potential range from −2.0 to 0 V.

3. Results and discussion

3.1. Structural analysis

The X-ray diffraction patterns of the prepared films of Ag_2CrO_4/SnS, bare Ag_2CrO_4 and bare SnS on FTO/AC films were recorded in the X-ray powder diffractometer (Bruker D8 ADVANCE ECO, 40 kV, 44 mA) between $20° < 2\theta < 80°$ at a grazing incident angle of 0.0027° using the Cu-Kα radiation ($\lambda = 1.54060$ Å).

As illustrated in Fig. 3 (a), the peaks attained for bare SnS film at the 2θ values of 25.93°, 27.47° and 31.56° can be indexed to the (120), (021) and (101) reflection planes that correspond to the orthohombic structure of SnS [30,31]. The dominant peak is at $2\theta \sim 31°$ suggesting SnS crystallites have preferred orientation along the (101) direction. No other impurity phases were observed in the XRD pattern indicating the formation of pure SnS film. For the Ag_2CrO_4 film, the peaks at 17.62°, 21.4°, 25.34°, 31.04°, 31.14°, 32.03°, 33.71°,35.07°, 37.03°, 39.26°, 42.57°, 44.26°, 44.50°, 48.05°, 50.26°, 52.07°, 52.07°, 55.84°, 57.07°, 61.93°, 62.60°, 64.95°, 66.48° and 66.70° match well with the orthorhombic Ag_2CrO_4 (JCPDS, No: 26–0952) and are well indexed without any impurity peaks as depicted in Fig. 3 (b). The preferential orientation was along the (031) plane indicating the maximum number of crystallites having the growth orientation along the (031) plane. Further, the shape of the diffraction peaks suggest that the products are well crystallized [32]. All peaks related to Ag_2CrO_4 and SnS in the XRD pattern of Ag_2CrO_4/SnS on FTO/AC film as shown in Fig. 3 (c) are in good resemblance with those of the bare Ag_2CrO_4 and bare SnS films. Furthermore, all peaks corresponding to orthorhombic SnS were found

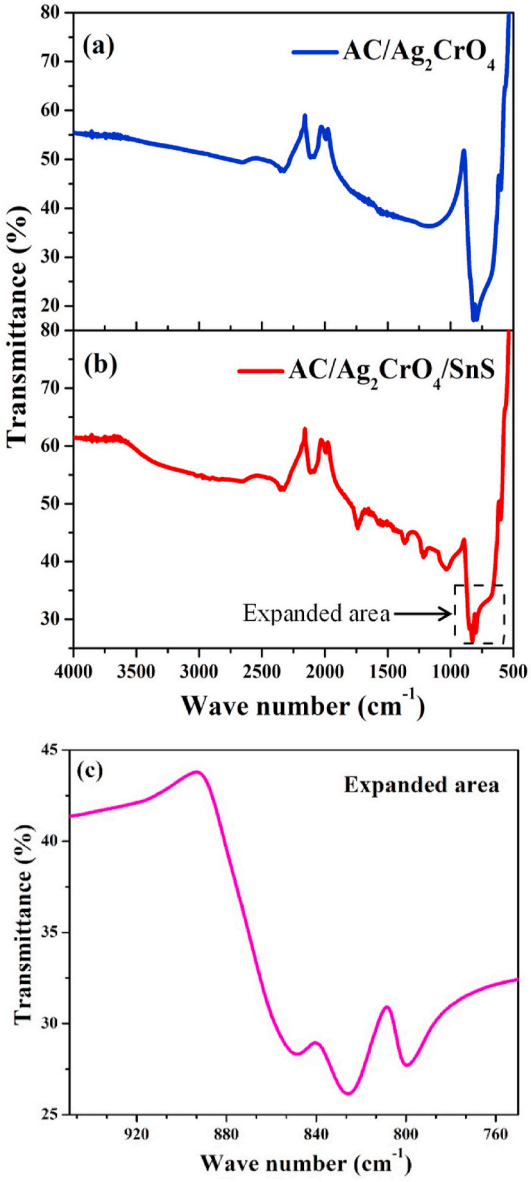

Fig. 5. FTIR spectra of **(a)** Ag_2CrO_4, **(b)** Ag_2CrO_4/SnS on FTO/AC films and **(c)** expanded FTIR spectra from 750 to 950 cm^{-1}.

in Ag_2CrO_4/SnS composite confirming incorporation of SnS filler in Ag_2CrO_4.

3.2. Surface microstructure analysis

The surface morphology of the synthesized films was analyzed using a scanning electron microscope (ZEISS SUPRA 55VP). The Scanning Electron Microscopic (SEM) images shown in Fig. 4 reveal the structure of Ag_2CrO_4 on AC coated FTO and particularly reflect the effect of SnS coating on FTO/AC/Ag_2CrO_4 films which has resulted in morphology changes. The rod-like morphology of the Ag_2CrO_4 nanoparticles as depicted in Fig. 4 (a) has changed into a flake-like morphology when SnS is heterostructured with the Ag_2CrO_4 as shown in Fig. 4 (b). The coating appears to be homogeneous throughout the surface of the FTO/AC films. The flake-like SnS has a well-defined shape with sharp edges. Fig. 4 (b) shown that the obtained product consists of a huge number of nano-flakes and densely packed.

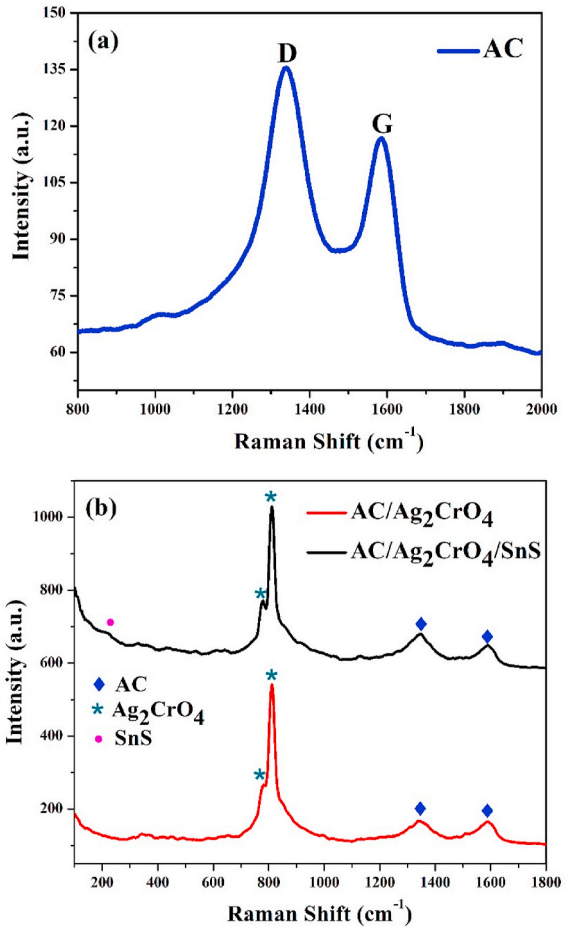

Fig. 6. Raman spectra of **(a)** AC on FTO **(b)** Ag_2CrO_4 and Ag_2CrO_4/SnS on FTO/AC films.

3.3. FTIR spectral analysis

The Fourier Transform Infrared Spectroscopy (FTIR, UNICAM 4600) was carried out in the wavelength range of 4000–500 cm^{-1} to identify the surface functional groups present in the prepared films. The FTIR spectra of Ag_2CrO_4, Ag_2CrO_4/SnS coated on FTO/AC films and expanded FTIR spectra of FTO/AC/Ag_2CrO_4/SnS film (750-950 cm^{-1}) were shown in Fig. 5. Fig. 5 (a) and **(b)** shows the strong absorption peaks of bare Ag_2CrO_4 at 856 and 830 cm^{-1} could be assigned to the stretching vibrations of Cr–O bonds in Ag_2CrO_4. The peaks for Ag_2CrO_4 are clearly shown in expanded FTIR spectra from 750 to 950 cm^{-1} [see the Fig. 5 (c)]. The appearance of the peaks located in between 900 and 1400 cm^{-1} which are due to the characteristics of SnS shown in Fig. 5 (b). Similar bands have also been observed in the FTIR spectra of SnS films reported in the literature [33,34]. However, peaks representing other binary phases of tin sulphide, like SnS_2 and Sn_2S_3, are not observed in the FTIR spectra, which confirm the results obtained by XRD. A minor peak observed in the range of 2000–2500 cm^{-1} in all the films may be due to the H–O–H bending vibration of water molecule. The presence of water in the synthesized materials could be attributed to the atmospheric moisture. All peaks related to Ag_2CrO_4 and SnS in the FTIR spectrum of Ag_2CrO_4/SnS film are in good resemblance with those of the bare Ag_2CrO_4 and bare SnS films.

3.4. Raman spectral analysis

Raman spectroscopy is an important and nondestructive technique which characterizes the structure and quality of carbon materials in the

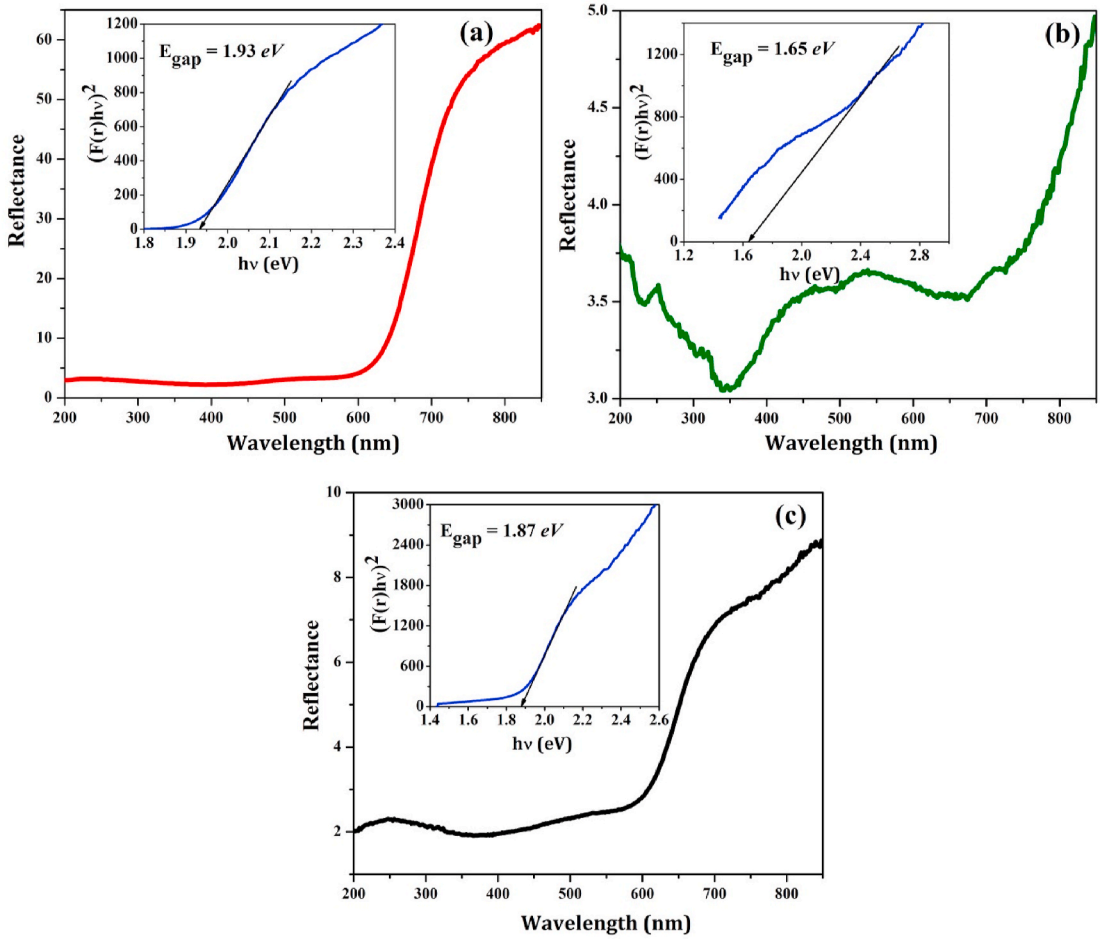

Fig. 7. Diffuse reflectance spectra and Kubelka-Munk plots of **(a)** bare Ag_2CrO_4 **(b)** bare SnS and **(c)** Ag_2CrO_4/SnS on FTO/AC films.

photoanodes. Fig. 6 represents the Raman spectra of AC on FTO, and Ag_2CrO_4 and Ag_2CrO_4/SnS on FTO/AC films. Fig. 6 (a) shows strong D and G bands approximately at 1340 and 1592 cm^{-1}, respectively, displaying the presence of amorphous carbon. The presence of D band in Raman scattering is associated with a disordered carbon structure. Further, sharp D bands in all the samples confirm that the AC does not contain graphite or graphene sheet structure. The two sharp bands observed at 780 and 816 cm^{-1} for Ag_2CrO_4 and Ag_2CrO_4/SnS, respectively on FTO/AC films may be attributed to the symmetric and asymmetric stretching vibrations of Cr–O bond in [CrO_4] clusters. Further, considerably weaker bands observed in the frequency region between 300 and 450 cm^{-1} for both Ag_2CrO_4 and Ag_2CrO_4/SnS on FTO/AC films may represent the bending vibrations of the CrO_4 group as shown in Fig. 6 (b). The active Raman band observed at 214 cm^{-1} reveals the presence of SnS in the Ag_2CrO_4/SnS on AC/FTO film. Similar Raman peaks have also been reported for Ag_2CrO_4 and SnS in literature [35–37].

3.5. Optical characterization

The diffuse reflectance spectroscopy (DRS, Thermo Scientific Evolution 600) was employed to study the light absorption ability of the prepared bare Ag_2CrO_4, bare SnS and Ag_2CrO_4/SnS on AC coated FTO films in the wavelength range from 200 to 850 nm and their spectra are displayed in Fig. 7 (a), (b) and **(c)**, respectively. The band gaps of the Ag_2CrO_4 and SnS nanoparticles were calculated according to the Kubelka–Munk (KM) method by the following equation.

$$[F(r)h\nu]^{1/n} = A(h\nu - E_g)^n \quad (1)$$

Where, F(r) is the Kulbelka-Munk function, E_g is the band gap energy, hν is the photon energy and A is a proportionality constant. In the above equation, n is a constant associated with different types of electronic transitions, such as n = 0.5 for direct allowed, n = 1.5 for direct forbidden, n = 2 for indirect allowed and n = 3 for indirect forbidden transitions [38,39]. The absorption edges for bare Ag_2CrO_4 and bare SnS on FTO/AC films are observed at 642.48 and 751.51 nm, respectively. Moreover, an intermediated absorption edge at 663.10 nm was observed for SnS coated Ag_2CrO_4 heterostructure film. The direct band gap energies of the films were calculated by extrapolating the linear region of $h\nu$ versus $[F(r)\ h\nu]^2$ plots using the equation (1) and found to be 1.93, 1.65 and 1.87 eV for bare Ag_2CrO_4, bare SnS and Ag_2CrO_4/SnS coated on FTO/AC films, respectively. The resulted band gap energies of bare Ag_2CrO_4 and bare SnS are similar to the literature values [40,41], whereas, Ag_2CrO_4/SnS seems to have an intermediated individual band gap energies of them.

3.6. Photoelectrochemical analysis

The photoelectrochemical properties of the working electrode were investigated by the cyclic voltammetry (CV) and electrochemical impedance spectroscopy (EIS) using the Bio Logic SP-150 potentiostat. Measurements were carried out with a three-electrode system to study the performance of the prepared electrode, and an aqueous solution buffered to pH 7 using a 0.1 M phosphate buffer solution was employed as the electrolyte. The electrodes were illuminated using a 150 W Xenon lamp for photoelectrochemical characterization, and the cyclic voltammetry was carried out in the potential range from −2.0 to 0 V.

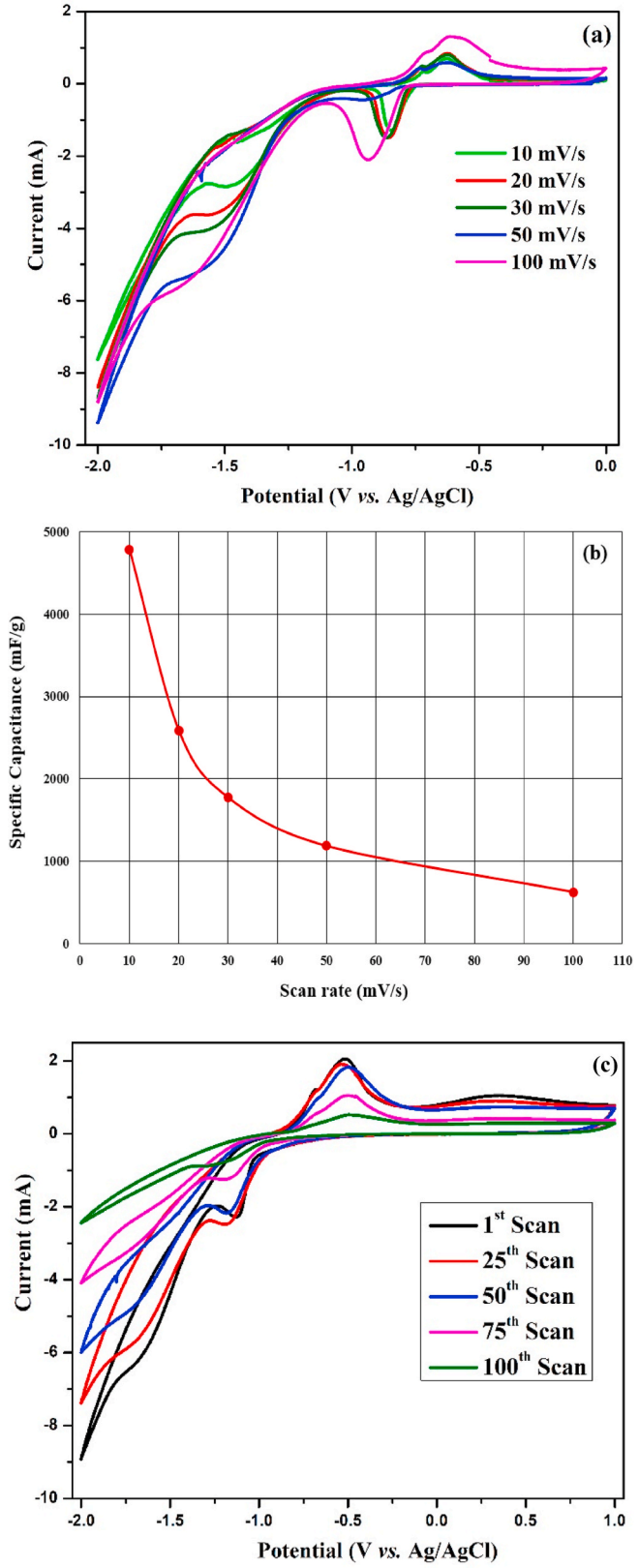

Fig. 8. (a) Cyclic voltammetry of FTO/AC/Ag_2CrO_4/SnS photoanode at different scan rates from 10 to 100 mV/s, **(b)** Plot of specific capacitance variation of the FTO/AC/Ag_2CrO_4/SnS photoanode as a function of scan rate and **(c)** Stability study of FTO/AC/Ag_2CrO_4/SnS photoanode at the scan rate of 100 mV/s.

Fig. 8 (a) depicts the CV curves of FTO/AC/Ag_2CrO_4/SnS photoanode at various scan rates from 10 to 100 mV/s (*vs.* Ag/AgCl). All the CV curves exhibit a pair of redox peaks suggesting that the capacitive characteristics are mainly governed by the faradaic redox mechanism, which is a sign of pesudocapacitive electrode nature [42]. The mechanism is based on the reversible redox reaction of $Sn\,(II) \leftrightarrow Sn\,(IV) + 2e^-$; the photoelectrochemical capacitance of FTO/AC/Ag_2CrO_4/SnS photoanode is attributed to the quasi reversible electron transfer process, which mainly involves the Sn^{2+}/Sn^{4+} redox couple, and probably mediated by the OH^- ions in the buffer electrolyte. Further, it is noteworthy that the shape of these CV curves barely changed as the scan rate increased, reflecting the good kinetic reversibility [43,44]. The FTO/AC/Ag_2CrO_4/SnS photoanode exhibited a CV curve with the maximum area covered at the scan rate of 10 mV/s, which may be due to the presence of AC and/or surface morphology of the as-prepared FTO/AC/Ag_2CrO_4/SnS photoanode.

The plot of the specific capacitance variation as a function of the scan rate of FTO/AC/Ag_2CrO_4/SnS photoanode in Fig. 8 (b) displays the obtained specific capacitances of 4782, 2591, 1775, 1187 and 628 mF/g at the scan rates of 10, 20, 30, 50 and 100 mV/s, respectively [29]. It is noted that the specific capacitance values get decreased when the scan rate increases, which is quite common in capacitors due to reduction in the available active sites with increasing scan rates.

Fig. 8 (c) illustrates the stability study of FTO/AC/Ag_2CrO_4/SnS photoanode at the scan rate of 100 mV/s. The shape of CV curve after 50 cycles of scanning was found to be similar to the original curve after first scan, indicating good photoelectrochemical stability. The intriguing capacitive behaviour of the as-prepared device is attributed to the integrated electrode materials with large surface area and synergistic effect of Ag_2CrO_4 and SnS. The highly conductive AC and Ag_2CrO_4 coated on the surface of SnS form conductive networks, and significantly accelerate electron and ion transport during charge-discharge processes at the photoanode. However, the specific capacitance of FTO/AC/Ag_2CrO_4/SnS photoanode is strictly depends on the structure (pore size and distribution) as well as surface area of the electrode materials.

The charge transfer process at the interface between electrode and electrolyte and the capacitive behaviour of FTO/AC/Ag_2CrO_4/SnS photoanode were comprehended by performing electrochemical impedance spectroscopic (EIS) analysis. Fig. S1 depicts the Nyquist plots obtained for the FTO/AC/Ag_2CrO_4/SnS photoanode under 1 sun illumination and in dark conditions are depicted in Fig. S1 (a) and **(b)**, respectively. The EIS analysis of the said photoanode revealed high resistance in dark, whereas a reduced resistance of ~275 Ω was attained with 1 sun illumination resulting in high energy storage/capacitance.

4. Conclusion

In this study, Ag_2CrO_4 and SnS nanoparticles were successfully prepared by ultrasonication and hydrothermal methods, respectively. Subsequently, the FTO/AC/Ag_2CrO_4/SnS photoanode was prepared by directly coating the as-prepared Ag_2CrO_4 and SnS powders on the AC coated FTO glass substrate. The XRD patterns of Ag_2CrO_4 and SnS confirmed orthohombic crystal structure. The observed rod-like surface morphology of Ag_2CrO_4 transformed into flake-like morphology when heterostructured with SnS. The FTIR and Raman spectral analyses further confirmed the structure and quality of the electrode materials. The diffuse reflectance spectra of Ag_2CrO_4 and SnS on FTO/AC sheet showed the band gap values of 1.93 and 1.65 eV respectively. The CV of FTO/AC/Ag_2CrO_4/SnS photoanode measured in the potential range from −2 to 0 V *vs* Ag/AgCl electrode at the scan rate of 10 mV/s showed a specific capacitance of 4782 mF/g when the device was subjected to visible light illumination (1 sun). The excellent capacitive property of the FTO/AC/Ag_2CrO_4/SnS heterostructured photoanode may be attributed to the porous structure of AC, which would have facilitated fast diffusion of ions and provided large active surface area for faradaic reactions, and the good conductivity of AC and Ag_2CrO_4. The remaining

limitation of the optimized Photocapacitor based on FTO/AC/Ag_2CrO_4/SnS photoanode arises from the higher resistance of PVDF binder that should be looked into in a future work. This study provides a promising route to the design of novel high efficiency energy storage materials and devices.

CRediT authorship contribution statement

Kajana Thirunavukarasu: Conceptualization, Methodology, Formal analysis, Software, Investigation, Validation, Data curation, Writing – original draft, Visualization. **Arumugam Pirashanthan:** Formal analysis, Software, Investigation, Validation, Data curation. **Akila Yuvapragasam:** Conceptualization, Methodology, Investigation, Validation, Data curation. **Dhayalan Velauthapillai:** Validation, Resources, Funding acquisition. **Punniamoorthy Ravirajan:** Validation, Resources, Funding acquisition. **Meena Senthilnanthanan:** Conceptualization, Methodology, Investigation, Validation, Data curation, Visualization, Resources. All authors have read and agreed to the published version of the manuscript.

Declaration of competing interest

The authors declare that they have no known competing financial interests or personal relationships that could have appeared to influence the work reported in this paper.

Acknowledgments

This work was supported by the Capacity Building and Establishment of Research Consortium (CBERC) [grant number LKA-3182-HRNCET] and Higher Education and Research collaboration on Nanomaterials for Clean Energy Technologies (HRNCET) [grant number NORPART/2016/10237] projects (http://project.jfn.ac.lk/hrncet/). The funding agencies had no role in the design of the study; in the collection, analyses, or interpretation of data; in the writing of the manuscript, or in the decision to publish the results.

Appendix A. Supplementary data

Supplementary data to this article can be found online at https://doi.org/10.1016/j.jpowsour.2021.230883.

References

[1] Z. Wang, J. Cheng, H. Huang, B. Wang, Flexible self-powered fiber-shaped photocapacitors with ultralong cyclelife and total energy efficiency of 5.1%, Energy Storage Mater. 24 (2020) 255–264, https://doi.org/10.1016/j.ensm.2019.08.011.

[2] T. Rajaramanan, M. Natarajan, P. Ravirajan, M. Senthilnanthanan, D. Velauthapillai, Ruthenium (Ru) Doped Titanium Dioxide (P25) electrode for dye sensitized solar cells, Energies 13 (2020) 1–13, https://doi.org/10.3390/en13071532.

[3] A. Pirashanthan, T. Murugathas, K. Mariappan, P. Ravirajan, D. Velauthapillai, S. Yohi, A multifunctional ruthenium based dye for hybrid nanocrystalline titanium dioxide/poly(3-hexylthiophene) solar cells, Mater. Lett. 274 (2020), 127997, https://doi.org/10.1016/j.matlet.2020.127997.

[4] A. Pirashanthan, T. Murugathas, N. Robertson, P. Ravirajan, D. Velauthapillai, A quarterthiophene-based dye as an efficient interface modifier for hybrid titanium dioxide/poly(3-hexylthiophene)(P3HT) solar cells, Polymers (Basel) 11 (2019) 1752, https://doi.org/10.3390/polym11111752.

[5] G. Timò, M. Calicchio, G. Abagnale, N. Armani, E. Achilli, M. Cornelli, F. Annoni, N. Castagnetti, M. Patrini, L.C. Andreani, L. Nasi, B. Schineller, Results on MOVPE SiGeSn deposition for the monolithic integration of III-V and IV elements in multi-junction solar cells, Sol. Energy Mater. Sol. Cells 224 (2021), 111016, https://doi.org/10.1016/j.solmat.2021.111016.

[6] A. Das, R.G. Nair, Fabrication of In_2O_3 functionalized ZnO based nanoheterojunction photoanode for improved DSSC performance through effective interfacial charge carrier separation, Opt. Mater. (Amst) (2021), 111784, https://doi.org/10.1016/j.optmat.2021.111784.

[7] C.-C. Hsu, S.-M. Yu, K.-M. Lee, C.-J. Lin, H.-C. Cheng, F.-R. Chen, Solid-state reaction process for high-quality organometallic halide perovskite thin film, Sol. Energy Mater. Sol. Cells 227 (2021), 111014, https://doi.org/10.1016/j.solmat.2021.111014.

[8] F. Mohamad, J. Teh, C.-M. Lai, Optimum allocation of battery energy storage systems for power grid enhanced with solar energy, Energy 223 (2021), 120105, https://doi.org/10.1016/j.energy.2021.120105.

[9] Q. Zeng, Y. Lai, L. Jiang, F. Liu, X. Hao, L. Wang, M.A. Green, Integrated photorechargeable energy storage system: next-generation power source driving the future, Adv. Energy Mater. 10 (2020) 1–30, https://doi.org/10.1002/aenm.201903930.

[10] P. Wang, X. Chen, G. Sun, C. Wang, J. Luo, L. Yang, J. Lv, Y. Yao, W. Luo, Z. Zou, A capacitor-type faradaic junction for direct solar energy conversion and storage, Angew. Chem. Int. Ed. 60 (2021) 1390–1395, https://doi.org/10.1002/anie.202011930.

[11] D. Schmidt, M.D. Hager, U.S. Schubert, Photo-rechargeable electric energy storage systems, Adv. Energy Mater. 6 (2016) 1–11, https://doi.org/10.1002/aenm.201500369.

[12] J. Zhang, Z. Wang, X. Li, J. Yang, C. Song, Y. Li, J. Cheng, Q. Guan, B. Wang, Flexible platinum-free fiber-shaped dye sensitized solar cell with 10.28% efficiency, ACS Appl. Energy Mater. 2 (2019) 2870–2877, https://doi.org/10.1021/acsaem.9b00207.

[13] G. Maddala, M. Ambapuram, V. Tankasala, R. Mitty, Optimal dye sensitized solar cell and photocapacitor performance with efficient electrocatalytic SWCNH assisted carbon electrode, ACS Appl. Energy Mater. 4 (2021) 11225–11233, https://doi.org/10.1021/acsaem.1c02087.

[14] S. Yun, Y. Qin, A.R. Uhl, N. Vlachopoulos, M. Yin, D. Li, X. Han, A. Hagfeldt, New-generation integrated devices based on dye-sensitized and perovskite solar cells, Energy Environ. Sci. 11 (2018) 476–526, https://doi.org/10.1039/C7EE03165C.

[15] W. Jin, M.M. Ovhal, H.B. Lee, B. Tyagi, J. Kang, Scalable, all-printed photocapacitor fibers and modules based on metal-embedded flexible transparent conductive electrodes for self-charging wearable applications, Adv. Energy Mater. 11 (2021), 2003509, https://doi.org/10.1002/aenm.202003509.

[16] N.K.C.S. Rout, Photo-powered integrated supercapacitors: a review on recent developments, challenges and future perspectives, J. Mater. Chem. A. 9 (2021) 8248–8278, https://doi.org/10.1039/D1TA00444A.

[17] T. Miyasaka, T.N. Murakami, The photocapacitor : an efficient self-charging capacitor for direct storage of solar energy 85 (2004) 3932–3934, https://doi.org/10.1063/1.1810630.

[18] S. Safshekan, I. Herraiz-Cardona, D. Cardenas-Morcoso, R. Ojani, M. Haro, S. Gimenez, Solar energy storage by a heterostructured $BiVO_4$–PbO_x photocapacitive device, ACS Energy Lett. 2 (2017) 469–475, https://doi.org/10.1021/acsenergylett.6b00728.

[19] X. Ren, X. Zhang, R. Guo, X. Li, Y. Peng, X. Zhao, X. Pu, Hollow mesoporous g-C_3N_4/Ag_2CrO_4 photocatalysis with direct Z-scheme: excellent degradation performance for antibiotics and dyes, Separ. Purif. Technol. 270 (2021), 118797, https://doi.org/10.1016/j.seppur.2021.118797.

[20] R. Biswas, S. Mete, M. Mandal, B. Banerjee, H. Singh, I. Ahmed, K.K. Haldar, Novel green approach for fabrication of Ag_2CrO_4/TiO_2/Au/r-GO hybrid biofilm for visible light-driven photocatalytic performance, J. Phys. Chem. C 124 (2020) 3373–3388, https://doi.org/10.1021/acs.jpcc.9b10866.

[21] N. Güy, M. Özacar, Ag/Ag_2CrO_4 nanoparticles modified on ZnO nanorods as an efficient plasmonic photocatalyst under visible light, J. Photochem. Photobiol. A Chem. 370 (2019) 1–11, https://doi.org/10.1016/j.jphotochem.2018.10.035.

[22] Y. Deng, L. Tang, G. Zeng, J. Wang, Y. Zhou, J. Wang, J. Tang, Y. Liu, B. Peng, F. Chen, Facile fabrication of a direct Z-scheme Ag_2CrO_4/g-C_3N_4 photocatalyst with enhanced visible light photocatalytic activity, J. Mol. Catal. A Chem. 421 (2016) 209–221, https://doi.org/10.1016/j.molcata.2016.05.024.

[23] K. Atacan, N. Güy, B. Boutra, M. Özacar, Enhancement of photoelectrochemical hydrogen production by using a novel ternary Ag_2CrO_4/GO/$MnFe_2O_4$ photocatalyst, Int. J. Hydrogen Energy 45 (2020) 17453–17467, https://doi.org/10.1016/j.ijhydene.2020.04.268.

[24] B. Peng, Y. Lu, J. Luo, Z. Zhang, X. Zhu, L. Tang, L. Wang, Y. Deng, X. Ouyang, J. Tan, J. Wang, Visible light-activated self-powered photoelectrochemical aptasensor for ultrasensitive chloramphenicol detection based on DFT-proved Z-scheme Ag_2CrO_4/g-C_3N_4/graphene oxide, J. Hazard Mater. 401 (2021), 123395, https://doi.org/10.1016/j.jhazmat.2020.123395.

[25] N. Shao, J. Wang, D. Wang, P. Corvini, Preparation of three-dimensional Ag_3PO_4/TiO_2@MoS_2 for enhanced visible-light photocatalytic activity and anti-photocorrosion, Appl. Catal. B Environ. 203 (2017) 964–978, https://doi.org/10.1016/j.apcatb.2016.11.008.

[26] Z. Liu, Y. Jiang, X. Liu, G. Zeng, B. Shao, Y. Liu, Y. Liu, W. Zhang, W. Zhang, M. Yan, X. He, Silver chromate modified sulfur doped graphitic carbon nitride microrod composites with enhanced visible-light photoactivity towards organic pollutants degradation, Compos. B Eng. 173 (2019), 106918, https://doi.org/10.1016/j.compositesb.2019.106918.

[27] Y. Ye, H. Yang, H. Zhang, J. Jiang, A promising Ag_2CrO_4/$LaFeO_3$ heterojunction photocatalyst applied to photo-Fenton degradation of RhB, Environ. Technol. (United Kingdom). 41 (2020) 1486–1503, https://doi.org/10.1080/09593330.2018.1538261.

[28] R.M. Abdelhameed, S.A. Al Kiey, A.R. Wassel, M. El-Shahat, Silver chromate doped Ti-based metal organic framework: synthesis, characterization, and electrochemical and selective photocatalytic reduction properties, New J. Chem. 45 (2021) 9526–9537, https://doi.org/10.1039/D1NJ00808K.

[29] T. Kajana, D. Velauthapillai, Y. Shivatharsiny, P. Ravirajan, A. Yuvapragasam, M. Senthilnanthanan, Structural and photoelectrochemical characterization of heterostructured carbon sheet/Ag_2MoO_4-SnS/Pt photocapacitor, J. Photochem.

Photobiol. A Chem. 401 (2020), 112784, https://doi.org/10.1016/j.jphotochem.2020.112784.
[30] J. Henry, K. Mohanraj, S. Kannan, S. Barathan, G. Sivakumar, Effect of selenium doping on structural and optical properties of SnS:Se thin films by electron beam evaporation method, Eur. Phys. J. Appl. Phys. 61 (2013), 10301, https://doi.org/10.1051/epjap/2012120359.
[31] A. Muthuvinayagam, T.M. David, P. Sagayaraj, Investigation on a one-pot hydrothermal approach for synthesizing high quality SnS quantum dots, J. Alloys Compd. 579 (2013) 594–598, https://doi.org/10.1016/j.jallcom.2013.07.108.
[32] J. Luo, X. Zhou, L. Ma, X. Xu, J. Wu, H. Liang, Enhanced photodegradation activity of methyl orange over Ag_2CrO_4/SnS_2 composites under visible light irradiation, Mater. Res. Bull. 77 (2016) 291–299, https://doi.org/10.1016/j.materresbull.2016.02.005.
[33] J. Tu, X. Shi, H. Lu, N. Yang, Y. Yuan, Facile fabrication of SnS_2 quantum dots for photoreduction of aqueous Cr (VI), Mater. Lett. 185 (2016) 303–306, https://doi.org/10.1016/j.matlet.2016.09.002.
[34] R. Kihal, H. Rahal, A.M. Affoune, M. Ghers, Electrodeposition of SnS thin film solar cells in the presence of sodium citrate, J. Electrochem. Sci. Technol. 8 (2017) 206–214, https://doi.org/10.5229/JECST.2017.8.3.206.
[35] D. Santamaría-Pérez, E. Bandiello, D. Errandonea, J. Ruiz-Fuertes, O. Gomis, J. A. Sans, F.J. Manjón, P. Rodríguez-Hernández, A. Muñoz, Phase behavior of Ag_2CrO_4 under compression: structural, vibrational, and optical properties, J. Phys. Chem. C 117 (2013) 12239–12248, https://doi.org/10.1021/jp401524s.
[36] G.S. Silva, L. Gracia, M.T. Fabbro, L.P. Serejo dos Santos, H. Beltrán-Mir, E. Cordoncillo, E. Longo, J. Andrés, Theoretical and experimental insight on Ag_2CrO_4 microcrystals: synthesis, characterization, and photoluminescence properties, Inorg. Chem. 55 (2016) 8961–8970, https://doi.org/10.1021/acs.inorgchem.6b01452.
[37] T.S. Reddy, M.C.S. Kumar, Co-evaporated SnS thin films for visible light photodetector applications, RSC Adv. 6 (2016) 95680–95692, https://doi.org/10.1039/c6ra20129f.
[38] A.F. Gouveia, J.C. Sczancoski, M.M. Ferrer, A.S. Lima, M.R.M.C. Santos, M.S. Li, R. S. Santos, E. Longo, L.S. Cavalcante, Experimental and theoretical investigations of electronic structure and photoluminescence properties of β-Ag_2MoO_4 microcrystals, Inorg. Chem. 53 (2014) 5589–5599, https://doi.org/10.1021/ic500335x.
[39] F.S. Cunha, J.C. Sczancoski, I.C. Nogueira, V.G. de Oliveira, S.M.C. Lustosa, E. Longo, L.S. Cavalcante, Structural, morphological and optical investigation of β-Ag_2MoO_4 microcrystals obtained with different polar solvents, CrystEngComm 17 (2015) 8207–8211, https://doi.org/10.1039/C5CE01662B.
[40] D. Sharma, N. Kamboj, K. Agarwal, B.R. Mehta, Structural, optical and photoelectrochemical properties of phase pure SnS and SnS_2 thin films prepared by vacuum evaporation method, J. Alloys Compd. 822 (2020), 153653, https://doi.org/10.1016/j.jallcom.2020.153653.
[41] D. Xu, S. Cao, J. Zhang, B. Cheng, J. Yu, Effects of the Preparation Method on the Structure and the Visible-Light Photocatalytic Activity of Ag_2CrO_4, 2014, pp. 658–666, https://doi.org/10.3762/bjnano.5.77.
[42] B. Jansi Rani, S.S. Pradeepa, Z.M. Hasan, G. Ravi, R. Yuvakkumar, S.I. Hong, Supercapacitor and OER activity of transition metal (Mo, Co, Cu) sulphides, J. Phys. Chem. Solid. 138 (2020), 109240, https://doi.org/10.1016/j.jpcs.2019.109240.
[43] K. Adib, E. Sohouli, M. Ghalkhani, H.R. Naderi, Z. Rezvani, M. Rahimi-Nasrabadi, Sonochemical synthesis of Ag_2WO_4/RGO-based nanocomposite as a potential material for supercapacitors electrodes, Ceram. Int. 47 (2021) 14075–14086, https://doi.org/10.1016/j.ceramint.2021.01.277.
[44] X. Zhao, Z. Li, Q. Guo, X. Yang, G. Nie, High performance organic-inorganic hybrid material with multi-color change and high energy storage capacity for intelligent supercapacitor application, J. Alloys Compd. 855 (2021), 157480, https://doi.org/10.1016/j.jallcom.2020.157480.